REGULAR ARTICLE

Role of step sites on water dissociation on stoichiometric ceria surfaces

Silvia Fuente · María M. Branda · Francesc Illas

Abstract The adsorption and dissociation of water on $CeO_2(111)$, $CeO_2(221)$, $CeO_2(331)$, and $CeO_2(110)$ has been studied by means of periodic density functional theory using slab models. The presence of step sites moderately affects the adsorption energy of the water molecule but in some cases as in $CeO_2(331)$ is able to change the sign of the energy reaction from endo- to exothermic which has important consequences for the catalytic activity of this surface. Finally, no stable molecular state has been found for water on $CeO_2(110)$ where the reaction products lead to a very stable hydroxylated surface which will rapidly become inactive.

Keywords Water gas shift · Ceria · CeO2 · DFT · GGA $+ U$

1 Introduction

Since the early forties, the water–gas shift reaction $(CO + H_2O \rightarrow CO_2 + H_2)$ constitutes an important step in the industrial production of CO-free hydrogen [1] to be subsequently used in hydrodesulfuration processes in oil

S. Fuente · F. Illas (✉)
Departament de Química Física and Institut de Química Teòrica i Computacional (IQTCUB), Universitat de Barcelona, C/Martí i Franquès 1, 08028 Barcelona, Spain
e-mail: francesc.illas@ub.edu

S. Fuente · M. M. Branda
Departamento de Física, Universidad Nacional del Sur, Bahía Blanca, Argentina

refineries, in ammonia synthesis through the Bosch–Haber process or in fuel cells [2]. The water–gas shift (WGS) reaction is also involved in other important industrial processes such as the methanol synthesis [3] or in the methanol steam reforming process [4]. In the chemical industry, the WGS reaction is carried out in two steps at high (623–673 K) and low (463–503 K) temperature [5]. The low temperature step uses Cu [6]- or Au [7–9]-based catalysts which often constitute the catalyst active phase [10–12]. Nevertheless, this apparently simple reaction is more complex that imagined and other factors must be considered such as the nature of the support [7, 13–16], the existence of point defect such as oxygen vacancies [17, 18], or the catalyst preparation process [19]. Likewise, subtle modifications of the catalyst by doping with traces of other metals [20, 21] or by formation of alloys [22, 23] have been found to considerably improve the catalytic performance. Nevertheless, the reaction mechanism, at least for the metallic phase and the low temperature step, is rather well understood, especially after a series of recent papers reporting microkinetic studies based mainly on the rate constants derived from density functional calculations [24–26] and the work of Fajin et al. [27] highlighting the important role of step sites.

Rather recently, inverse catalysts where an inactive noble metal surface such as Au(111) acts as support for CeO_2 or TiO_2 nanoparticles have proven to be active for the WGS reaction and almost as good catalysts as Cu extended surfaces [23, 28]. X-ray photoelectron spectroscopy (XPS) and scanning tunneling microscopy (STM) experiments [23] suggest that the catalytic activity of these systems toward the WGS reaction is strongly related to the direct participation of the oxide–metal interface in the catalytic process. Moreover, these experiments have shown that water can easily dissociate on either $TiO_{2-x}/Au(111)$

or CeO_{2-x}/Au(111) but that no water dissociation is seen when there are no O vacancies in the supported oxide nanoparticles. These findings are in agreement with surface science experiments showing strong adhesion of molecularly adsorbed water to stoichiometric CeO_2(111) [29] and further surface reduction when reduced CeO_{2-x}(111) was exposed to water with a concomitant presence of hydroxyl groups [30, 31] and are also in agreement with theoretical studies based on density functional calculations for the stoichiometric CeO_2(111) and reduced CeO_{2-x}(111) surfaces indicating that water does not dissociate on the clean surface, whereas the process becomes thermodynamically favorable on the oxygen vacancies containing surface [32–34].

From the discussion above, one can readily see that comparison between the experiments for the inversed catalyst models and the surface science systems coincides in evidencing the important role of the oxygen vacancies on the catalyzed dissociation of water. However, one must also realize that the ceria nanoparticles supported on Au(111) in the inverse catalysts necessarily posses a large number of edge-like sites which are not present in either the CeO_2(111) or the CeO_{2-x}(111) surfaces. It is reasonable to argue that the presence of low-coordinated sites will somehow influence the reactivity of these systems toward water dissociation. This is especially the case since it has been suggested that the presence of step edges can lead to the appearance of Ce^{3+} centers even without the presence of oxygen vacancies [35].

The interaction of water with ceria surfaces has been the object of several theoretical studies although all consider the CeO_2(111) surface only. Thus, Fronzi et al. [32] considered water adsorption on stoichiometric and reduced CeO_2(111) surfaces using the standard PBE, pure GGA functional, which is adequate for the stoichiometric surface but questionable for the reduced one. They found that the most stable configuration for water is when the O atoms is bonded directly to a Ce surface cation and involving two H-bonds between the hydrogen atoms and the surface oxygen atoms. The adsorption energy reported by these authors for the stoichiometric surface is -0.49 eV. Clearly, the adsorption energy of water appears to be stronger when oxygen vacancies are present although this is not considered in the present work. These authors also find that water does not spontaneously dissociate on the clean stoichiometric surface, while on the surface with oxygen vacancies, this process becomes thermodynamically favorable. A smaller value of the adsorption energy (-0.35 eV) for water on the perfect CeO_2(111) stoichiometric surface was reported by Watkins et al. [36] but, as noticed by Fronzi et al. [32], this is because the equilibrium geometry configuration obtained by these authors is not the most stable one, the reason being the existence of only one hydrogen bond between the adsorbed molecule and the ceria surface.

Hence, the reason behind this discrepancy can be attributed to the difficulty to locate the most stable adsorption. Note also that different choices of surface unit cell induce different lateral interactions among the adsorbates and to a strong dependence of the binding energy with respect to the coverage. More recently, Yang et al. [37, 38] studied the interaction of a water molecule with the (111) surfaces of stoichiometric and reduced ceria using DFT $+$ U. For the stoichiometric surface, their results are similar to those of Fronzi et al. [32] and also coincide with the results of Kumar et al. [15] and also of Chen et al. [39] using PW91 and PW91 $+$ U, respectively.

In order to investigate the role of low coordinated step sites in the dissociation of water catalyzed by ceria without interfering with possible effects derived from the size of the nanoparticles, such as their size dependence facility to promote oxygen vacancy formation [40], a series of density functional calculations have been carried out to establish the energy profile of water dissociation on CeO_2(111), CeO_2(221), CeO_2(331), and CeO_2(110) which have been found to be, in this order, the most stable surfaces [41]. We will show that the presence of low-coordinated sites has a moderate influence on the energy barrier for water dissociation except for the later which is found to be especially reactive.

2 Computational details

Self-consistent density functional theory (DFT) calculations using slab periodic models with large enough supercells have been carried out to study the adsorption and dissociation of H_2O on the regular CeO_2(111), (221), (331), and (110) surfaces. The calculations have been carried out using the PW91 [42, 43] form of the Generalized Gradient Approximation (GGA) corrected with the so called Hubbard parameter (U) [44]. The one-electron wave functions are expanded in a basis of periodic plane waves with a cut-off of 415 eV for the kinetic energy. The PAW method [45] in the implementation of Kresse and Joubert [46] was used to represent the effect of the inner cores on the valence density. The integration in the Brillouin zone was performed on a proper Monkhorst–Pack grid [47] of $5 \times 5 \times 1$ special k-points. The total energy tolerance defining self-consistency of the electron density was 10^{-4} eV. The structures of the system under study were optimized until the maximum forces acting on each atom became less than 0.01 eV/Å. All density functional calculations were carried out with the *Vienna* Ab Initio *Simulation Package* (VASP) [48–51].

The introduction and choice of the numerical value for the U parameter deserves a further comment. It penalizes the double occupation of *4f* orbital and thus allows for a

proper description of reduced ceria [52–54]. In the present work, a value of $U = 4$ eV has been chosen on the basis of previous experience and several considerations. Note that this value is slightly larger than the value of 3 eV proposed [54] to achieve a sufficiently balanced description of both CeO_2 and Ce_2O_3 but closer to the value of $U = 5$ eV suggested by other authors [52, 53, 55]. In addition, $U = 4$ eV has been found to be necessary to properly describe localized solutions for Ce^{3+} cations in ceria nanoparticles [40, 56–59] and, also, largely facilitates convergence toward self-consistency of the Kohn–Sham equations. In the following, we will use the notation G4 to indicate DFT calculations carried out with the PW91 implementation of GGA and using an effective U value of 4 eV.

The perfect CeO_2(111), (221), (331), and (110) surfaces were represented by slabs models and proper unit cells. However, the size of the unit cell depends on the type of surface and also on the size and shape of the adsorbed molecule and the dissociation fragments. Thus, to model the stepped CeO_2(221) and (331) surfaces, it is necessary to employ slab models with larger number of layers. Therefore, 2×2, 4×2, 3×2, and 4×2 units cells with 3, 8, 6, 4 layers of CeO_2 units (three atomic layers each) have been used to represent the CeO_2(111), (221), (331), and (110) surfaces, respectively. Using this slab models, the minor distance between adsorbed water molecules is 7.7 Å. Therefore, we can consider that the initial adsorbed molecules and the final dissociated fragments on the surface do not interact. A vacuum width larger than 10 Å was used to avoid interaction between the periodically repeated slabs. A water molecule has been added to each surface mode and the resulting structure obtained from total energy minimization, a similar relaxation procedure has been used to obtain the structure of dissociated water molecule fragments (H and OH). In all cases, the outermost external layers of the CeO_2 were fully relaxed, i.e., 1, 2, 2, and 1 layers of CeO_2 units for CeO_2(111), (221), (331), and (110) surfaces, respectively. The transition state structures have been located using the climbing image nudged elastic band (CI-NEB) method of Henkelman et al. [60, 61]. The stable configuration of the adsorbed molecules and the TS structures was characterized by appropriate vibrational analysis.

Once the optimum geometries for the reactants and products have been obtained and the transition state structure characterized, calculations for a representative set, these structures have been also carried out allowing spin polarization. In all cases, the calculations converged to the non-spin polarized solution. Consequently, the analysis of results in the next section is based always on the results of non-spin polarized calculations.

3 Results and discussion

3.1 Water molecular adsorption on ceria surfaces

Here, we discuss the results for molecular water adsorption on the different surfaces studied in the present work. The adsorption energy is calculated as

$$E_{ads} = E(H_2O/CeO_2) - E(H_2O) - E(CeO_2) \qquad (1)$$

where negative energies indicate an exothermic process. For the stoichiometric CeO_2(111) surface, the present results coincide almost quantitatively with those of Fronzi et al. [32]. Thus, the present estimate for E_{ads} from G4 calculations differs only 0.03 eV (Table 1) from those reported Fronzi et al. [32] using PBE, which is a pure GGA functional and is within 0.01 eV of those reported by Chen et al. [39] using a similar (PW91 + U; $U = 6.3$) approach. The agreement between the different sets of calculations suggests that, in fact, the introduction of the U term is not necessary as far as no oxygen vacancies (i.e., Ce^{3+} cations) are present.

From the preceding discussion, it appears that the description of the interaction of water with the stoichiometric CeO_2(111) surface provided by different density functional approaches and slightly different surface models is almost the same excepting perhaps the results of Watkins et al. [36] although the reason for the discrepancy is also understood (see above). In addition, the calculated value of the adsorption energy compares well with experimental estimate of 0.53 eV for 0.2 ML coverage arising from thermal programmed desorption data for CeO_2 thin films grown on ytria stabilized zirconia [62], and it is not far from the 0.61 eV value obtained from CeO_2 powders [63]. Therefore, one may expect a similarly accurate prediction

Table 1 Relevant structural data and adsorption energy (E_{ads}) of H_2O on the ceria (111), (221), and (331) surfaces and note that no stable molecular adsorption state has been found for water on the (110)

Surface	d_{O-Ce} (Å)	d_{O-H} (Å)	$d_{O(sup)-H}$ (Å)	$\angle HOH$ (°)	E_{ads} (eV)
(111)	2.62	0.99/0.98	2.03/2.10	107.5	−0.52
(221)	2.68	0.99/0.98	2.06/2.18	107.8	−0.56
(331)	2.64	0.99/0.98	1.98/2.33	106.8	−0.72

for the rest of ceria surfaces considered in the present work. Results for the (221) and (331) in Table 1 indicate that the adsorption energy of water does only moderately depend on the crystal face. For the (221) surface, it is only slightly larger than for the most stable (111) surface, and going to the (331) surface does only increase E_{ads} up to 0.72 eV which, interestingly enough, is close to the thermodynamic heat of adsorption measured for CeO_2 powders. The closeness between the calculated values for the adsorption energy of water on these three surfaces strongly suggests that the bonding mode is very similar. This is indeed the case as one can see from the structural data reported in Table 1 and the corresponding structures in Fig. 1. Note that the structure of adsorbed water is almost the same in the three surfaces and that the only difference is the slight difference in the distance from the O atom to the Ce surface atom.

The case of the CeO_2(110) surface deserves a separate discussion since all attempts to locate a stable molecularly adsorbed state have been unsuccessful. In fact, all geometry optimization calculations converged to a situation where the water molecule is spontaneously dissociated into OH and H (see next section). This result seems to be rather surprising since there is no experimental evidence of water dissociation on ceria unless oxygen vacancies are present. However, one may argue that this is because ceria samples used in the experiments have predominantly (111) facets which are rather unreactive. A different situation may
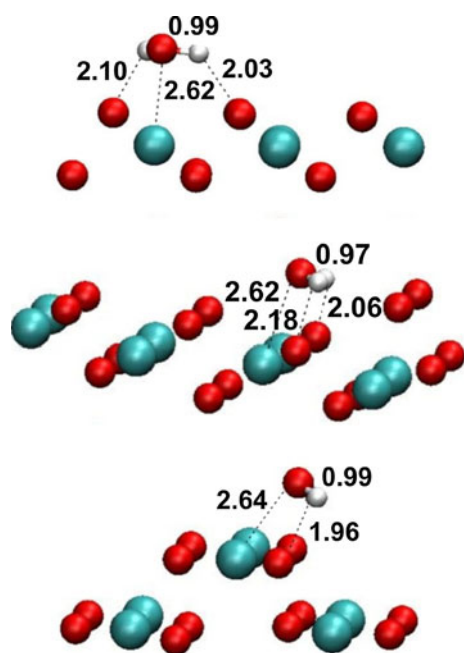
Fig. 1 Schematic representation of the structure of the most stable configuration of water adsorbed on the (111), (221), and (331) ceria surfaces (*top*, *middle* and *bottom panels*, respectively). The interatomic distances are expressed on Å

occur if samples with other more reactive crystal planes can be synthesized. This has been precisely the approach followed by Zhou et al. [64]. These authors have used a solution-based hydrothermal method to obtain single crystalline CeO_2 nanorods exhibiting dominantly (100) and (110) surfaces. These authors show that these nanorods are more reactive for CO oxidation that ceria nanoparticles with more stable terminations. In the view of the present results, one may speculate that these types of crystals are active toward water dissociation. However, it is also likely that the resulting systems will not lead to good catalysts because the surface, even initially active toward water dissociation, will become rapidly deactivated because of the extremely strong binding of the reaction products as it will be further commented in the next section. The resulting surface will become fully hydroxylated and chemically inactive. Note that the catalytic activity of these special ceria nanorods obtained from wet chemistry requires the precipitate to be filtrated, washed with deionized water, dried at 60 °C for 24 h, and then calcined at 350 °C for 4 h [64]. It is also worth mentioning that very recently Yang et al. succeeded in synthesizing ceria nanoparticles exposing either (111) or (100) faces [65].

3.2 Water dissociation on ceria surfaces

In order to discuss the molecular mechanism of water dissociation on the different well-defined surfaces of stoichiometric ceria considered in the present work, we have first determined the most stable sites for the coadsorption of H and OH (see Fig. 2) and used these and the structure of adsorbed water to run the CI-NEB calculations and thus locate the corresponding transition state (TS) structures. From these calculations, it has been possible to construct the energy profiles. The relevant energy data were reported in Table 2. In particular, we focus on the activation (E_{act}) and reaction (E_{reac}) energy which are defined as in Eqs. 2 and 3

$$E_{act} = E(H_2O/CeO_2)_{TS} - E(H_2O/CeO_2) \qquad (2)$$

$$E_{reac} = E(H + OH/CeO_2) - E(H_2O/CeO_2) \qquad (3)$$

with this definition positive activation energy values indicate an energy barrier and negative reaction energy values indicate that the process is exothermic. Finally, we consider the adsorption energy of the dissociation products (E'_{ads}) as

$$E'_{ads} = E(H + OH/CeO_2) - E(H_2O) - E(CeO_2). \qquad (4)$$

Let us start by considering the most stable, and also more studied, CeO_2(111) surface. The reaction is predicted to be slightly endothermic (Table 2) and, hence, the reaction products, H and OH adsorbed on top of a surface
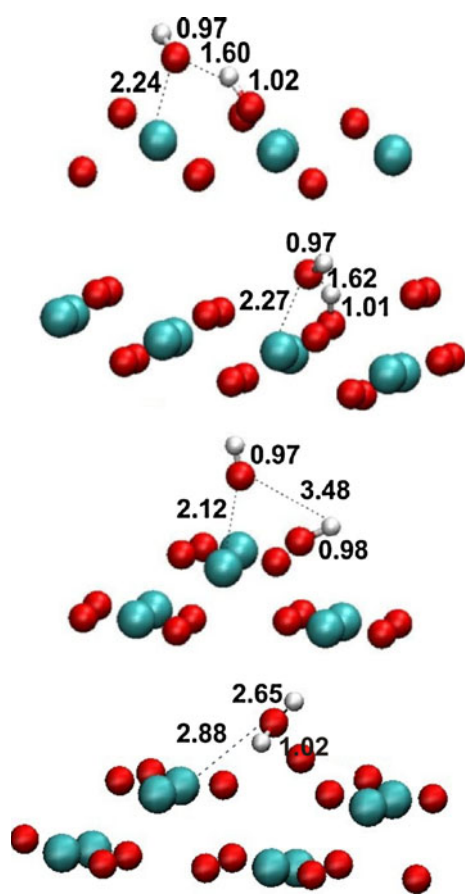
Fig. 2 Schematic representation of the structure of the dissociated water adsorbed on the (111), (221), (331), and (110) ceria surfaces from *top* to *bottom*, respectively. The interatomic distances are expressed on Å

Table 2 Activation (E_{act}), reaction (E_{reac}), and H + OH coadsorption (E'_{ads}) energy (in eV) for water dissociation on several ceria surfaces

Surface	E_{act}	E_{reac}	E'_{ads}
(111)	+0.19	+0.14	−0.38
(221)	+0.31	+0.27	−0.29
(331)	+0.21	−0.14	−0.86
(110)	–	–	−4.57

oxygen and of a surface ceria, respectively, are to some extent less stable than adsorbed water. On this surface, water dissociation faces a moderate energy barrier of 0.19 eV which is significantly lower than the desorption energy indicating that the process could take place. However, the presence of the energy barrier requires an extra energy cost. Consequently, water dissociation will not be facilitated, in agreement with the experimental observation that water does not spontaneously dissociate on this surface unless oxygen vacancies are present [23, 28]. From the data on Table 2, one can also see that even if the energy barrier

to dissociate water on this surface can be overcome at a moderately high temperature, the inverse reaction will be faster orders of magnitude since the corresponding energy barrier is of 0.05 eV only. Note that the energy barrier for water dissociation on this stoichiometric surface is noticeably smaller than the one reported by Fronzi et al. [32] for the reduced $CeO_{2-x}(111)$ surface. These authors report a value larger than 2 eV for reduced which is against the experimental evidence that dissociation of water on this surface. Note also that for the stoichiometric surface, the present values for E_{ads} and E_{reac} are almost identical to those reported by Fronzi et al. which leads us to conclude that the algorithm used by these authors to locate the TS converged to a wrong structure. Finally, one must realize that the activation energy reported by these authors is significantly larger than the desorption energy (1.28 eV) reported in the same work.

Let us now focus on the stepped surfaces which allow us to investigate in detail the role of the low-coordinated edge site. For the $CeO_2(221)$ surface, the situation is similar to the (111) surface and it even appears to be less reactive. Thus, the energy barrier is slightly larger but, again smaller than water adsorption energy on this surface, and the reaction is also slightly more endothermic. In this case, the presence of step sites does not largely changes the reactivity, probably because the presence of step edges does only destabilize the surface to a rather small extent, and the atomic structure of adsorbed water, coadsorbed H and OH and transition state for water dissociation are also very similar indicating also that the chemical bond between these two ceria surfaces and these adsorbates has a strong local character. Next, we consider the $CeO_2(331)$ surface which is only moderately less stable than the previous one. However, the rather subtle change in atomic structure and surface stability has a more pronounced effect on the molecular mechanism for water dissociation. In fact, the reaction is now predicted to be fairly exothermic which is consistent with the larger adsorption of molecular water. In any case, the additional thermodynamic driving force for the dissociation reaction does not appear to be enough to facilitate it. In fact, the calculated activation energy is only 0.02 eV larger than the value predicted for the most stable $CeO_2(111)$ surface. However, the fact that the reaction is now exothermic has implications for the reverse step. Now, assuming that the system receives (e.g., by heating) the energy necessary to overcome the barrier for water dissociation, the reaction will proceed because the reverse step has now to surmount an energy barrier of 0.35 eV. Therefore, one can conclude that this type of stepped stoichiometric surface has the potential to act as a rather good catalyst for water dissociation, for instance in the WGS reaction. There is, of course, the difficulty to prepare it but the recent advances in synthetic methods already

allow to grow ceria nanoparticles with preferential (111) or (100) facets [65]. It is then likely than nanoparticles with (331) could be also obtained.

Finally, we consider the case of the $CeO_2(110)$ surface where all attempts to locate a molecularly adsorbed state for water have failed and lead to the situation where the molecule spontaneously splits. The resulting products, H and OH, are strongly bound to the surface with an adsorption energy of 4.57 eV (Table 2) which indicates that once the water molecule is broken, a very stable hydroxylated surface will be formed which from now on will be chemically inactive. This high surface activity could be attributed to the specific position that O and Ce atoms occupy on this surface. In fact, in this case, both Ce and O surface atoms are located at the same outermost atomic layer (see Fig. 1 of [41]). This allows the simultaneous formation of strong Ce_{sup}–OH and O_{sup}–H bonds and thus facilitates water dissociation. This interpretation is consistent with the fact that the topmost atomic layer of the least active (111) surface exposes only oxygen atoms favoring the formation of O_{sup}–H bonds but difficulting the interaction of OH species with the surface. On the other hand, (221) and (331) surfaces show also oxygen atoms on the top layer but here atoms at the step edges provide the necessary Ce and O surface sites.

4 Conclusions

The adsorption and dissociation of water on the four most stable surfaces of stoichiometric ceria has been studied by means of periodic density functional theory using slab models. The analysis of the energy profile for the corresponding molecular mechanism allows us to extract important conclusions about the role of step sites in this important chemical reaction. In particular, present values for the stoichiometric surfaces provide a valuable reference for further modeling of reduced surfaces where experiment indicate that the process occurs spontaneously and, hence, necessarily with energy barriers smaller than those corresponding to the stoichiometric surfaces studied in the present work.

The presence of step sites does only moderately affect the adsorption energy of the water molecule which varies from −0.52 eV for $CeO_2(111)$ to −0.72 eV for $CeO_2(331)$. However, molecular water does not seem to be stable on the CeO2(110) surface where spontaneous dissociation is predicted. In agreement with the results for water adsorption energy, the energy barrier for water dissociation exhibits little variation with the crystal face. The calculated values for the energy barrier are roughly of 0.2 eV, and hence, one can argue that it may be easily surmounted by moderate heating of the system. However, for the (111) and

(221) surfaces, the reaction is predicted to be endothermic, and consequently, the energy barrier for the recombination of adsorbed H and OH is smaller than that corresponding to water dissociation, and consequently, even if energy is provided to the system so that water molecules could dissociate, recombination will be much faster making the process completely inefficient from a catalytic point of view. A different situation occurs on the $CeO_2(331)$ surface. Here, the reaction is moderately exothermic; the energy barrier for water dissociation is similar to the one calculated for the other two surfaces but the recombination step faces now a higher energy barrier. Consequently, the stoichiometric $CeO_2(331)$ surface could act as a reasonable good catalyst for water dissociation. Finally, no stable molecular state has been found for water on $CeO_2(110)$. Nevertheless, this surface cannot be considered as catalytically active since the reaction products lead to a very stable hydroxylated surface which will rapidly become inactive.

The prediction that $CeO_2(331)$ can result in a catalytically active surface is appealing although at present the interest is mainly academic. Recent advances in the synthesis of ceria nanoparticles or nanorods with defined crystal faces [63, 64] will perhaps allow to experimentally verify this prediction and may open the way toward a new family of designed catalysts.

References

1. Ladebeck JR, Wagner JP (2003) Handbook of fuel cells—fundamentals, technology and applications (ISBN: 0-471-49926-9). Vielstich W, Lamm A, Gasteiger HA (eds), vol 3, Part 2: 190–201. Wiley, Chichester
2. Lee SHD, Applegate DV, Ahmed S, Calderone SG, Harvey TL (2005) Int J Hydrogen Energy 30:829–842
3. Rozovskii AY, Lin GI (2003) Top Catal 22:137–150
4. LarrubiaVargas MA, Busca G, Costantino U, Marmottini F, Montanari T, Patrono P, Pinzari F, Ramis V (2007) J Mol Catal A Chem 266:188–197
5. Newsome DS (1980) Catal Rev Sci Eng 21:275–315
6. Schumacher N, Boisen A, Dahl S, Gokhale AA, Kandoi S, Grabow LC, Dumesic JA, Mavrikakis M, Chorkendorff I (2005) J Catal 229:265–275
7. Burch R (2006) Phys Chem Chem Phys 8:5483–5500
8. Mendes D, Garcia H, Silva VB, Mendes A, Madeira LM (2009) Ind Eng Chem Res 48:430–439
9. Rodríguez JÁ, Evans J, Graciani J-B, Park J, Liu P, Hrbek J, Sanz JJF (2009) Phys Chem C 113:7364–7370

10. Li L, Zhan Y, Zheng Q, Zheng Y, Lin X, Li D, Zhu J (2007) Catal Lett 118:91–97
11. Boccuzzi F, Chiorino A, Manzoli M, Andreeva D, Tabakova T (1999) J Catal 188:176–185
12. Liu Z-P, Jenkins SJ, King DA (2005) Phys Rev Lett 94:196102 (1–7)
13. Yahiro H, Murawaki K, Saiki K, Yamamoto T, Yamaura H (2007) Catal Today 126:436–440
14. Rodríguez JA, Liu P, Hrbek J, Pérez M, Evans J (2008) J Mol Catal A: Chem 281:59–65
15. Kumar P, Idem R (2007) Energy Fuels 21:522–529
16. Rodriguez JA, Liu P, Wang X, Wen W, Hanson J, Hrbek J, Pérez M, Evans J (2009) Catal Today 143:45–50
17. Wang X, Rodríguez JA, Hanson JC, Gamarra D, Martínez-Arias A, Fernández-García MJ (2006) Phys Chem B 110:428–434
18. Chen Y, Cheng J, Hua P, Wang H (2008) Surf Sci 602:2828–2834
19. Zhang L, Wang X, Millet J-MM, Matter PH, Ozkan US (2008) App Catal A Gen 351:1–8
20. Du X, Yuana Z, Cao L, Zhanga C, Wanga S (2008) Fuel Processing Technol 89:131–141
21. Nishida K, Atake I, Li D, Shishido T, Oumi Y, Sano T, Takehira K (2008) App Catal A Gen 337:48–57
22. Knudsen J, Nilekar AU, Vang RT, Schnadt J, Kunkes EL, Dumesic JA, Mavrikakis M, Besenbacher FJ (2007) Am Chem Soc 129:6485–6490
23. Zhao X, Ma S, Hrbek J, Rodriguez JA (2007) Surf Sci 601:2445–2452
24. Liu P, Rodriguez JA (2007) J Chem Phys 126:164705–164712
25. Gokhale AA, Dumesic JA, Mavrikakis M (2008) J Am Chem Soc 130:1402–1414
26. Madon RJ, Braden D, Kandoi S, Nagel P, Mavrikakis M, Dumesic JA (2011) J Catal 281:1–11
27. Fajin JLC, Cordeiro MNDS, Illas F, Gomes JRB (2009) J Catal 268:131–141
28. Rodriguez JA, Ma S, Liu P, Hrbek J, Evans J, Pérez M (2007) Science 318:1757–1760
29. Gritschneder S, Iwasawa Y, Reichling M (2007) Nanotechnology 18:044025–044030
30. Henderson MA, Perkins CL, Engelhard MH, Thevuthasan S, Peden CHF (2003) Surf Sci 526:1–18
31. Berner U, Schierbaum K, Jones G, Wincott P, Haq S, Thornton G (2000) Surf Sci 467:201–213
32. Fronzi M, Piccinin S, Delley B, Traversa E, Stampfl C (2009) Phys Chem Chem Phys 11:9188–9199
33. Yang Z, Wang Q, Wei S, Ma D, Sun Q (2010) J Phys Chem C 114:14891–14899
34. Yang Z, Xie L, Ma D, Wang G (2011) J Phys Chem C 115:6730–6740
35. Branda MM, Loschen C, Neyman KM, Illas F (2008) J Phys Chem C 112:17643–17651
36. Watkins MB, Foster AS, Shluger AL (2007) J Phys Chem C 111:15337–15341
37. Yang Z, Wang Q, Wei S, Ma D, Sun Q (2010) J Phys Chem C 114:14891–14899
38. Yang Z, Xie L, Ma D, Wang GJ (2011) Phys Chem C 115:6730–6740
39. Chen H-T, Choi YM, Liu M, Lin MC (2007) Chem Phys Chem 8:849–855
40. Migani A, Vayssilov GN, Bromley ST, Illas F, Neyman KM (2010) Chem Commun 46:5936–5938
41. Branda MM, Ferullo RM, Causà M, Illas F (2011) J Phys Chem C 115:3716–3721
42. Perdew JP, Chevary JA, Vosko SH, Jackson KA, Pederson MR, Singh DJ, Fiolhais C (1992) Phys Rev B 46:6671–6687
43. Perdew JP, Chevary JA, Vosko SH, Jackson KA, Pederson MR, Singh DJ, Fiolhais C (1993) Phys Rev B 48:4978
44. Dudarev SL, Botton GA, Savrasov SY, Humphreys CJ, Sutton AP (1998) Phys Rev B 57:1505–1509
45. Blöchl PE (1994) Phys Rev B 50:17953–17979
46. Kresse G, Joubert D (1999) Phys Rev B9(59):1758–1775
47. Monkhorst HJ, Pack JD (1976) Phys Rev B 13:5188–5192
48. Kresse G, Hafner J (1993) Phys Rev B 47:558–561
49. Kresse G, Hafner J (1993) Phys Rev B 48:13115–13118
50. Kresse G, Hafner J (1994) Phys Rev B 49:14251–14269
51. Kresse G, Furthmuller J (1996) Phys Rev B 54:11169–11186
52. Nolan M, Grigoleit S, Sayle DC, Parker SC, Watson GW (2005) Surf Sci 576:217–229
53. Fabris S, de Gironcoli S, Baroni S, Vicario G, Balducci G (2005) Phys Rev B 71:041102 (1–4)
54. Loschen C, Carrasco J, Neyman KM, Illas F (2007) Phys Rev B 75:035115 (1–8)
55. Lu Z, Yang Z (2010) J Phys: Condens Matter 22:475003 (1–10)
56. Loschen C, Migani A, Bromley ST, Illas F, Neyman KM (2008) Phys Chem Chem Phys 10:5730–5738
57. Migani A, Loschen C, Illas F, Neyman KM (2008) Chem Phys Lett 465:106–109
58. Migani A, Neyman KM, Illas F, Bromley ST (2009) J Chem Phys 131:64701 (1–7)
59. Migani A, Vayssilov GN, Bromley ST, Illas F, Neyman KM (2010) J Mater Chem 20:10535–10546
60. Henkelman G, Uberuaga BP, Jonsson H (2000) J Chem Phys 113:9901–9904
61. Henkelman G, Jonsson H (2000) J Chem Phys 113:9978–9985
62. Henderson MA, Perkins CL, Engelhard MH, Thevuthasan S, Peden CHF (2003) Surf Sci 526:1–18
63. Prin M, Pijolat M, Soustelle M, Touret O (1991) Thermochim Acta 186:273–283
64. Zhou K, Wang X, Sun X, Peng Q, Li Y (2005) J Catal 229:206–212
65. Yang F, Choi Y, Agnoli S, Liu P, Stacchiola DJ, Hrbek J (2011) Rodriguez J A J Phys Chem C 115:23062–23066